Redox-Sensitive PEG-Polypeptide Nanoporous Particles for Survivin Silencing in Prostate Cancer Cells

Francesca Cavalieri[a,b], *Giovanni L. Beretta*[c], *Jiwei Cui*[a], *Julia A. Braunger*[a], *Yan Yan*[a], *Joseph J. Richardson*[a], *Stella Tinelli*[c], *Marco Folini*[c], *Nadia Zaffaroni**[c] *and Frank Caruso**[a]

[a]ARC Centre of Excellence in Convergent Bio-Nano Science and Technology, and the Department of Chemical and Biomolecular Engineering, The University of Melbourne, Parkville, Victoria 3010, Australia

[b]Dipartimento di Scienze e Tecnologie Chimiche Università di Roma Tor Vergata, Via della ricerca scientifica 1 00173, Roma, Italy

[c]Department of Experimental Oncology and Molecular Medicine, Fondazione IRCCS Istituto Nazionale dei Tumori Via G. Amadeo, 42 – 20133 Milano, Italy

KEYWORDS: siRNA delivery, PEG-poly-L-lysine, redox-responsive particles, SIM, FLIM imaging.

ABSTRACT: We report the engineering of intracellular redox-responsive nanoporous poly(ethylene glycol)-poly(L-lysine) particles (NPEG-PLLs). The obtained particles exhibit no toxicity while maintaining the capability to deliver a small interfering RNA sequence (siRNA) targeting the anti-apoptotic factor, survivin, in prostate cancer cells. The redox-mediated cleavage of the disulfide bonds stabilizing the NPEG-PLL-siRNA complex results in the release of bioactive siRNA into the cytosol of prostate cancer PC-3 cells, which in turn leads to the effective silencing (~59 ± 8%) of the target gene. These findings, obtained under optimal conditions, indicate that NPEG-PLLs may protect the therapeutic nucleic acid in the extracellular and intracellular environment, thus preventing the occurrence of competitive interactions with serum and cytosolic proteins, as well as degradation by RNase. The intracellular trafficking and final fate of the NPEG-PLLs were investigated by a combination of deconvolution microscopy, fluorescence lifetime imaging microscopy and super-resolution structured illumination microscopy. A significant impairment of cell survival was observed in cells concomitantly exposed to paclitaxel and siRNA-loaded NPEG-PLLs. Overall, our findings indicate that NPEG-PLLs represent a highly loaded depot for the delivery of therapeutic nucleic acids to cancer cells.

INTRODUCTION

Small interfering RNA (siRNA) delivery systems are a potential new class of nanomedicines that can selectively silence disease-causing genes.[1-3] Although promising for cancer treatment, the low bioavailability of siRNA has hampered their translation into clinical use. Typically, due to their net negative charge and relatively large size, synthetic siRNA does not readily cross biological barriers. In addition, siRNA duplexes are quickly degraded by serum and intracellular ribonucleases. As a consequence, efficient systemic delivery necessitates the use of suitable carriers to physically protect siRNA therapeutics and facilitate their cellular uptake, while still maintaining their functionality. Because of their passive tumor targeting ability,[4] nanoparticles are desirable delivery vehicles for cancer therapy. However, both micrometer and nanometer-sized carriers are suitable for siRNA delivery depending on the specific target tissue. For instance, immunotherapy of kidney or pancreas cancers, melanomas, or other solid tumors requires the effective delivery of siRNA by micron- or sub-micron sized vectors to blood mononuclear cells or dendritic cells.[5] For example, treatment of lung-associated diseases by siRNA rely on the use of particles with aerodynamic diameters of 1-10 μm.[6] Hence, a number of siRNA-based vectors have been developed, such as micelles,[7] polyion complexes (PIC),[8,9] polymeric nanoparticles,[10,11] and metal-organic frameworks (MOFs).[12]

Cationic biomaterials, including polymers, lipids, polysaccharides, cell penetrating peptides, and dendrimers are particularly suitable for siRNA packaging and for *in vitro* delivery, because they condense siRNA into complexes with a positive surface charge, promoting endocytosis by electrostatically adsorbing onto anionic cell membranes.[13] However, the *in vitro* stability of the polycation-siRNA complex is compromised by dilution, ionic strength and the competitive

binding of serum proteins. Systemic administration of micelle-siRNA complexes resulted in the dissociation of the complex and a short blood half-life (5 min).[7] Recently, many approaches have been proposed to overcome the poor stability of PICs. TAT modified chitosan/siRNA complexes were used to silence luciferase (about 70%) in MCF-7 with 200 nM siRNA.[11] PEGylated nanogels, composed of quaternized polyamine with enhanced siRNA binding affinity, have shown 50% gene silencing activity in human hepatocarcinoma (HuH-7 cells) using 200 nM siRNA.[14] Anti-survivin siRNA was complexed with PEG-pp-PEI-PE (polyethylene glycol-peptide-polyethylenimine-1,2-dioleoyl-*sn*-glycero-3-phosphoethanolamine) and transferred into human Non-Small Cell Lung Cancer, NSCLC, cells, resulting in survivin down-regulation for about 30% of cells at 150 nM siRNA.[15] It is worth noting that the gene silencing effect observed in these recent studies is strongly dependent on the siRNA concentration and high siRNA doses (150-300 nM) are transfected *in vitro*, which indicates a low transfection efficiency for the systems.

Downregulation of survivin up to 80 % was demonstrated by using non-degradable caprylic acid-substituted polyethylenimine (PEI).[16] In this study a low siRNA dose (54 nM) was transfected *in vitro* in MDA-MB-231 cells for 72 h. PEI has been extensively investigated for siRNA delivery because PEI is a potent *in vitro* carrier due to its high cellular uptake and endosomolytic activity.[17]

Recently, we reported a templated assembly technique for replica particle formation using mesoporous silica (MS) particles as sacrificial templates.[18] Porous templates such as MS and calcium carbonate particles have porous interiors that can be used to encapsulate compounds with a high loading capacity.[19-21] In the present paper, we used this technique for the engineering

of intracellular redox-responsive nanoporous poly(ethylene glycol)-poly-L-lysine particles, NPEG-PLLs, for the efficient and safe release of a low dose of siRNA (31 nM) designed to target the anti-apoptotic factor survivin in prostate cancer cells. Survivin is a protein highly expressed in the majority of malignant tumors compared to normal tissues.[22] It is a member of the Inhibitor of Apoptosis Protein (IAP) family, thus acting as a suppressor of apoptosis and favoring tumor progressions.[23,24] In addition, it has been widely demonstrated that the over-expression of survivin causes resistance to radiation and chemotherapeutic agents, and it has been reported to correlate with poor prognosis in cancer patients.[22] Several strategies, such as small molecules, peptidomimetic and antisense oligomers (including siRNA) have been reported to suppress survivin expression in cancer.[22] However, the available therapeutic approaches have yielded only partial positive responses in clinical trials because of the inefficient *in vivo* delivery and poor bioavailability of naked siRNA. In this context, our NPEG-PLLs offer a positively charged nanoporous template to entangle negatively charged anti-survivin siRNA, while the PEG chains provide a redox-responsive crosslinker to stabilize the nanoporous carriers against dilution and competitive serum protein binding. Our study demonstrates that NPEG-PLLs may effectively protect siRNA from the adverse conditions of the extracellular and intracellular environment. The exposure of prostate cancer cells to survivin-directed siRNA, delivered through NPEG-PLLs along with a low dose of paclitaxel, resulted in improvement of the cytotoxic activity of the anticancer drug. This feature highlights the potential of this carrier to become a support for therapeutic intervention for cancer treatment.

EXPERIMENTAL SECTION

Materials. Poly(-L-lysine) (M_w 60 kDa), chloroquine (30 mg L^{-1}), protease from *Streptomyces griseus, dithiothreitol* (DTT), dextran-FITC (M_w 500 and 2000 kDa), FITC were purchased from Sigma-Aldrich (St. Louis, MO) and used as received. The PEG–NHS disulfide crosslinker was purchased from Santa Cruz Biotechnology, Inc. Alexa Fluor 488 carboxylic acid, succinimidyl ester (AF488-NHS) was obtained from Life Technologies (Australia). PicoGreen was supplied by Molecular Probes (Eugene, OR). Scrambled siRNA (siScr; sense 5'-GGU CGU CGG CUA CUU CUA CTT, antisense 5'-GUA GAA GUA GCC GAC GAC CTT, and siSurv (sense 5'-GGA CCA CCG CAU CUC UAC ATT, antisense 5'-UGU AGA GAU GCG GUG GUC CTT), targeting specific consensus sequences [5'-AA(N19)UU-3'] within the survivin mRNA (Genbank accession no. NM_001168.1) where synthesized by eurofins MWG Operon. 5'-AF488 siRNA was synthesized by QIAGEN.

The human prostate PC-3 carcinoma cell lines were obtained from American Type Culture Collection. Cells were resuscitated soon after arrival, and grown as a monolayer in RPMI 1640 containing 10% fetal bovine serum (FBS). All cultures were maintained at 37 °C in a humidified 5% CO_2 incubator. Roswell Park Memorial Institute medium (RPMI1640), FBS, phosphate buffered saline (PBS), sodium dodecyl sulfate (SDS) and trypsin were obtained from BioWhittaker (Verviers, Belgium). The primary antibodies, polyclonal to survivin (rabbit), polyclonal to LC3 (rabbit), monoclonal to β-actin (mouse), were obtained from Abcam (Cambridge, UK), Cell signaling (Danvers, MA) and Sigma-Aldrich (UK), respectively. The anti-mouse and anti-rabbit horseradish peroxidase-linked secondary antibodies (Life Technologies Europe BV, Monza, Italy), and the ECL western blotting detection reagents were obtained from GE Healthcare (Milano, Italy). Opti-MEM, FBS and Lipofectamine2000 were

purchased from Life Technologies. High-purity (Milli-Q) water used in all experiments was prepared by a Millipore Milli-Q water purification system with a resistivity greater than 18 MΩ·cm.

Preparation and Characterization of NPEG-PLLs. NPEG-PLL were prepared via the MS templating method.[19,20] Briefly, 3 mg of MS particles was washed with phosphate buffer (100 mM, pH 8) and incubated in 600 μL of PLL solution (5 mg mL^{-1} in phosphate buffer) under constant shaking for at least 4 h. Subsequently, the particles were isolated by centrifugation (1500 rcf, 1 min) and washed three times with phosphate buffer. The pellet was redispersed in 100 μL of PEG-NHS-disulfide crosslinker (5 mg mL^{-1}). After at least 2 h incubation, the particles were labeled with AF488-NHS. The MS templates were then dissolved with a buffered hydrofluoric acid (HF) solution (2 M HF/8 M NH_4F, 300 μL, pH ~5), followed by three washing steps. *Caution! HF is highly toxic. Extreme care should be taken when handling HF solution and only small quantities should be prepared.* The PLL content of a single NPEG-PLL was determined to be 0.6 pg/particle by using AF488-labeled PLL (0.3% DS) to prepare fluorescent AF488-NPEG-PLL. After preparation, an aliquot of 10 μL of AF488-NPEG-PLL suspended in PBS was dissolved in 140 μL 10 mM DTT for 4 h. A calibration curve correlating the fluorescence intensity of AF488 PLL solutions and their corresponding concentrations (from 0.02 mg mL^{-1} to 0.3 mg mL^{-1}) was developed to quantify the amount of PLL in a single particle. The experiments were performed in triplicate. Zeta (ζ)-potential measurements of NPEG-PLLs and siRNA-loaded NPEG-PLLs in 10 mM NaCl were carried out using a Malvern Zetasizer. For the transmission electron microscopy (TEM) analysis, 3 μL of NPEG-PLLs were allowed to adsorb onto a carbon-coated Formvar film mounted on 300-mesh copper grids (ProSciTech,

Australia). After blotting dry, the grids were air dried overnight and then analyzed using TEM (Philips CM120 BioTWIN) operated at 120 kV. To determine the pore size, NPEG-PLLs were incubated in 0.5 mg mL^{-1} M_W 500 kDa and M_W 2000 kDa FITC-dextran for 30 min in PBS at room temperature, washed twice with PBS and analyzed by confocal laser scanning microscopy (CLSM), using a Leica TCS SP2 confocal system equipped with an HCX PL APO lbd.BL 63× 1.4 NA oil objective. The images were then analyzed using ImageJ software. Potentiometric titration analysis was applied to determine the amine and carboxyl groups content of the NPEG-PLLs and to estimate the degree of particle crosslinking. NPEG-PLLs (0.3-1 mg) was dispersed in 0.5 mL of 0.15 M NaCl, and the pH of the suspension was initially adjusted to 11 using 0.1 N NaOH. Next, the suspension was titrated with 8 mM HCl to pH 3. PLL dissolved in 0.15 M NaCl, and 0.15 M NaCl solutions were titrated in the same way as controls. To determine the carboxyl/amine groups ratio, NPEG-PLLs were dispersed in 0.5 mL of 0.15 M NaCl and the suspension initially adjusted to pH 3 using 0.1 N HCl. The suspension was titrated to pH 11 using 4 mM NaOH. The pH of the solutions was measured after each addition by a pH meter (microprobe Mettler-Toledo, Inc. Columbus OH).

Determination of NPEG-PLL Crosslinking Degree. The crosslinking degree of NPEG-PLL was determined by equilibrium swelling experiments applying the Flory Rehner theory (eqn (1)) that was recently applied to the determination of microgels structure[25]:

$$\frac{\upsilon e}{Vo} = -\frac{\frac{1}{V_1}\left[\ln(1-\varphi_{2s}) + \varphi_{2s} + \chi\varphi_{2s}^2\right]}{\varphi_{2r}\left[\left(\left(\frac{\varphi_{2s}}{\varphi_{2r}}\right)^{1/3}\right) - \frac{1}{2}\left(\frac{\varphi_{2s}}{\varphi_{2r}}\right)\right]}$$

where $\frac{\upsilon e}{Vo}$ is the crosslinks density ($molcm^{-3}$), χ is the Flory polymer-solvent thermodynamic interaction parameter, V_1 is the molar volume of water, φ_{2s} is the equilibrium swollen polymer

volume fraction measured in 0.2 M NaCl, and φ_{2r} is the relaxed polymer volume fraction. φ_{2s} and φ_{2r} were evaluated taking into account the polymer mass per particles and NPEG-PLL diameter in the swollen and dry state. The extent of swelling depends on crosslinking the degree, the concentration of ionic groups within the network, the degree of ionization of PLL, and the electrolyte concentration in solution. As the swelling of NPEG-PLLs was carried out in 0.2 M NaCl, the ionic osmotic pressure difference between the particle interior and exterior became reduced and the swelling controlled only by the neutral component of the network.[26] A weighted average was used to calculate a value of χ=0.44 (based on mole fractions of PLL and PEG) repeat units in the NPEG-PLL.[27]

Post Loading of siRNA into NPEG-PLLs. An aliquot of 10 μL of NPEG-PLLs (1.3×10^7 particles μL^{-1}) was incubated in DNase/RNase free 0.5 X PBS buffer with 10 μL of siRNA (7.7 μM) for 30 min, centrifuged and washed several times in PBS. The siRNA or AF488-siRNA uptake into the NPEG-PLLs was measured using a NanoDrop spectrophotometer by recording the absorbance at 260 nm or 495 nm of the solutions before and after adsorption taking into account the absorbance of three washing steps. The number of NPEG-PLLs per microliter (1.3×10^7 NPEG-PLL μL^{-1}) in the sample was quantified using flow cytometry.

Thermal Stability of siRNA-Loaded NPEG-PLLs. The thermal denaturation of the released siRNA was analyzed after NPEG-PLL degradation by protease. An aliquot (10 μL) of protease from *Streptomyces griseus* dissolved in PBS buffer (1 mg mL^{-1}) was incubated at 37 °C overnight with 50 μL of NPEG-PLLs (1.3×10^7 particles μL^{-1}). To follow the siRNA thermal denaturation, PicoGreen, a double-stranded selective dye, was used to fluorescently stain the

duplex and the fluorescence intensity of the intercalated dye was measured using a Horiba Yvon-Jacob FL3–22 fluorimeter as a function of temperature. PicoGreen has an excitation maximum at 480 nm and an emission maximum at 520 nm. An aliquot of 1 µL siRNA (21 µM) was diluted to 250 µL PBS buffer and 0.5 µL PicoGreen (3.2 µM). The fluorescence emission of the mixture was recorded in the range 20-80 °C. The thermal denaturation of the released siRNA was analyzed after NPEG-PLL degradation by protease.

***In Vitro* Serum and Plasma Stability of siRNA-Loaded NPEG-PLLs.** The serum stability of AF488-siRNA loaded into NPEG-PLLs was characterized using a NanoDrop spectrophotometer. AF488-siRNA-loaded NPEG-PLLs were incubated for 4 h in PBS pH 7.4 containing 10% FBS and for 3 h in human plasma K_2 EDTA. After centrifugation, the siRNA displaced from NPEG-PLL by serum proteins was evaluated by measuring the absorbance at 495 nm of the supernatant and subtracting the background absorbance. To evaluate the colloidal stability of NPEG-PLLs in plasma, 7×10^7 AF488-siRNA-loaded NPEG-PLLs were incubated with human plasma K_2 EDTA for 48 h. Samples were monitored by confocal microscopy to assess whether the plasma protein adsorbed onto NPEG-PLL promoted particle aggregation. The adsorption of plasma protein on the NPEG-PLL surface was verified by ζ-potential measurements.

***In Vitro* Glutathione**, **GSH, and Protease-Induced Degradation of NPEG-PLLs.** An aliquot of 10 µL of NPEG-PLL (1.3×10^7 particles μL^{-1}) was added to 140 µL of GSH solution and incubated up to 6 h at 37 °C. The suspension of NPEG-PLLs was centrifuged and the supernatant analyzed by using TECAN fluorescence microplate reader for different incubation times. An aliquot (10 µL) of protease from *Streptomyces griseus* dissolved in PBS buffer (1 mg mL^{-1}) was incubated at 37 °C overnight with 50 µL of NPEG-PLLs (1.3×10^7 particles uL^{-1}). After

incubation the suspension was analyzed by fluorescence microscopy. Fluorescence microscopy images of degraded NPEG-PLLs were acquired using an inverted Olympus IX71 microscope (60× oil objective lens, 488 nm excitation filter). A black and white camera mounted on the left port of the microscope was used to capture the microscopy images.

Cell Viability Assay. Cell viability was assessed by the MTS (3-(4,5-dimethylthiazol-2-yl)-5-(3-carboxymethoxyphenyl)-2-(4-sulfophenyl)-2H-tetrazolium) assay (CellTiter 96® AQueous One Solution Cell Proliferation Assay, Promega, Milano, Italy), according to the manufacturer's protocol. Briefly, cells were seeded at 2000 cells/well into 96-well plates. The following day, the cells were treated with NPEG-PLLs (50-1000 particles/cell) for 96 h in a final volume of 100 µL of standard growth medium (2.2-44 µg polymer/mL). At the end of the treatment, 20 µL of MTS (3-(4,5-dimethylthiazol-2-yl)-5-(3-carboxymethoxyphenyl)-2-(4-sulfophenyl)-2H-tetrazolium salt) solution was added to each well. MTS is converted to formazan by mitochondrial dehydrogenases present in metabolically active cells, and the reaction is directly proportional to the number of viable cells. Untreated cells were set as a negative control, and cells treated with $HgCl_2$ were used as a positive control. The absorbance was recorded using the FLUOstar OPTIMA plate reader (BMG Labtech GmbH, Offenburg, Germany) at 492 nm after 4 h incubation at 37 °C in 5% CO_2.

Flow Cytometry. PC-3 cells were seeded in 6-well plates for 24 h. Cells were then treated with AF488-labeled NPEG-PLLs at a particle/cell ratio of 72:1 or 125:1 for different time intervals at 37 °C and 5% CO_2. After the treatment (specifically, 0, 6, 16 and 24 h), cells were washed with PBS three times and harvested by trypsinization followed by centrifugation at 400 *g* for 5 min.

The cell pellet was resuspended in PBS and analyzed by flow cytometry (Partec Cyflow Space, Partec GmbH, Germany). Cells that were associated with NPEG-PLLs were identified in the FL5 fluorescence channel of the flow cytometer.

Deconvolution Microscopy. PC-3 cells were plated into 8-well Lab-Tek I chambered coverglass slides (Thermo Fisher Scientific, Rochester, NY) and allowed to adhere overnight. Cells were then incubated with AF488-labeled NPEG-PLLs (125 particles/cell) for 24 h (37 °C, 5% CO_2). After three washes with PBS, cells were fixed with 4% paraformaldehyde for 20 min at room temperature, permeabilized with 0.1% Triton X-100 in PBS for 5 min, and blocked with 1% BSA in PBS for 5 min. Samples were then incubated for 1 h with mouse anti-human LAMP1 monoclonal antibody (2.5 μg mL^{-1}) in PBS containing 0.25% BSA) (BD Pharmingen, San Diego, CA) followed by detection with AF647-labeled goat anti-mouse IgG (2 μg mL^{-1} in PBS containing 0.25% BSA) (Life Technologies) for 1 h at room temperature. Optical sections were collected using a fluorescence deconvolution microscope (Applied Precision, USA). Colocalization analysis was performed with Imaris software (Bitplane AG, Zürich, Switzerland).

Super-Resolution Structured Illumination Microscopy (SIM). PC-3 cells were cultured as described for the deconvolution experiments. Cells were then incubated with AF488-NPEG-PLLs (125 particles/cell) for 1 h (37 °C, 5% CO_2) followed by three washes with standard growth medium to remove non-internalized particles. After 120 h incubation (37 °C, 5% CO_2), the cells were fixed, permeabilized and immunostained as described for the deconvolution microscopy experiments. Mouse anti-human LAMP1 monoclonal antibody and AF568-labeled

goat anti-mouse IgG were applied at the same concentrations to visualize the lysosomes, while the nuclei were stained with Hoechst 33342.

LAMP1 is the lysosomal-associated membrane protein 1 which localizes on the lysosomal membrane. We used a fluorescently-labeled antibody recognizing this protein in order to visualize lysosomes and the colocalization between nanovectors and lysosomes.

Vectashield was used as mounting medium (Vector Laboratories, USA). SIM experiments were carried out with an Applied Precision DeltaVision OMX V4 Blaze Structured Illumination Microscope using an Olympus 60×, 1.24 NA oil objective, 405 nm, 488 nm, and 568 nm laser illumination, and standard excitation and emission filter sets. Raw images were acquired at a 125-nm z-step size, aligned and reconstructed in three dimensions with softWoRx 6.1.3 (Applied Precision) software.

Fluorescence Lifetime Imaging Microscopy (FLIM). PC-3 cells were cultured as described for the deconvolution experiments. FITC-labeled NPEG-PLLs were added to cells at a particle/cell ration of 500:1 and incubated for 1 h (37 °C, 5% CO_2) followed by three washes with standard growth medium to remove non-internalized particles. Cells were then incubated (37 °C, 5% CO_2) and imaged at specific time points (0.5, 2, 6, 24 and 48 h). The fluorescence lifetime of FITC-NPEG-PLL was analyzed via Time-Correlated Single Photon Counting (TCSPC)–FLIM using an inverted confocal microscope (Leica TCS SP2). To excite FITC-NPEG-PLL, a pulsed 405 nm laser diode (PicoQuant) at a repetition rate of 10 MHz and an acquisition range of 500-600 nm was used and data was recorded according to the manufacturer's recommendations (Leica D FLIM; http://www.becker-hickl.de/leicaman.htm). SPCImage software was employed to measure fluorescence lifetimes and to process lifetimes decay curves and imaging.

Delivery of siSurv into PC-3 Cells by NPEG-PLLs. PC-3 cells were seeded at a density of 100 000 cells per well in a 6-well plate. A cell density of about 10,500 cells/cm^2 was used. 24 h after seeding, transfection with Lipofectamine2000 was performed using a 31 nM final concentration of siRNA. Freshly prepared NPEG-PLLs loaded with siRNA (31 nM) were delivered to PC-3 cells (1000 particles/cell) using a method similar to that used for standard transfection. Briefly, NPEG-PLLs filled with siRNA or Lipofectamine2000/siRNA complex were incubated with cells in Opti-MEM serum-free medium. The amount of Lipofectamine2000 used for transfection experiments in 6-well plates complies with the protocol purchased by the company (20 pg/cell). After 4 h of transfection, the standard growth medium containing 10% FBS was added. Cells were incubated at 37 °C, 5% CO_2 for 72 or 120 h, and then harvested for successive analyses.

Western Immunoblotting Assay of PC-3 Cells Treated with NPEG-PLLs. Total protein extracts from PC-3 cells treated with NPEG-PLLs were prepared according to standard methods.[28] 40 μg of protein extracts were fractioned by SDS polyacrylamide gel electrophoresis and transferred to nitrocellulose using standard protocols. The membranes were blocked with PBS containing 5% (w/v) skim milk and incubated overnight with anti-survivin, anti-LC3 primary antibodies. The membranes were then incubated with secondary anti-mouse and anti-rabbit peroxidase-linked whole antibodies. Bound antibodies were detected using the Novex ECL, HRP Chemiluminescent substrate Reagent Kit. Filters were autoradiographed and images were acquired using a BioSpectrum Imaging System (Ultra-Violet Products Ltd, Cambridge, UK). An anti-β-actin monoclonal antibody (Abcam) was used on each blot to ensure equal loading of protein on the gel.

***In Vitro* Gene Silencing and Treatment with Paclitaxel by Using NPEG-PLLs**. Briefly, 24 h after seeding in 48-well plates, PC-3 cells were exposed for 120 h to freshly prepared NPEG-PLLs filled with siRNA (1000 particles/cell). Particles were incubated with cells in Opti-MEM serum-free medium for 4 h of transfection. Then, cells were not washed and standard growth medium containing 10% FBS was added. After 72 h treatment with particles, paclitaxel (30 nM) was added for the last 48 h. Cells were collected and counted in a particle counter (Coulter Counter, Coulter Electronics, Luton, UK). Each experimental sample was run in triplicate.

RESULTS AND DISCUSSION

NPEG-PLL Synthesis and Chemical Characterization. The redox-sensitive NPEG-PLLs were prepared by infiltrating PLL into MS particles followed by PLL crosslinking using PEG-N-hydroxy-succinimide-disulfide linkers (PEG-NHS-disulfide) (Supporting Information, Figure S1), and subsequent removal of the MS templates (Scheme 1). MS particles with a bimodal pore structure (smaller mesopores in the 2–3 nm range and larger mesopores between 10–40 nm)[19,20] were used as templates. A PEG-NHS disulfide crosslinker was selected to introduce redox sensitive crosslinking into the NPEG-PLLs. The rationale for using a redox-responsive polymeric drug delivery system is the significant difference in redox potentials between extracellular and intracellular environments. It has been reported that in the cytosol and nuclei the concentration of glutathione (GSH), the most abundant redox agent in mammalian cells, can reach 10 mM, whereas outside the cell, the concentration drops to approximately 2-20 μM.[29] Hence, NPEG-PLLs are designed to preserve the particle integrity in the oxidizing bloodstream, whereas in a intracellular environment the particles are subjected to high GSH concentrations,

which is expected to promote cargo release. In addition, it is noted that the proteolytic activity in the extracellular environment is negligible; hence, NPEG-PLLs can be potentially degraded only by lysosomal proteases. The amount of infiltrated PLL (0.2 mg g^{-1} of MS) was determined by monitoring the difference in the AF488-PLL fluorescence in solution before and after adsorption. The PLL mass of a single NPEG-PLL (0.6 pg/particle) after dissolution of the template was determined by quantifying the amount of AF488-PLL in an aliquot of NPEG-PLLs using a UV-vis calibration curve and flow cytometry to count the number of particles suspended in the aliquot. The residual content of amine groups after crosslinking was evaluated by potentiometric titration of NPEG-PLL suspension (Supporting Information, Figure S2a).

Scheme 1. Schematic Illustration of siRNA Encapsulation into NPEG-PLL via Mesoporous Silica Templating

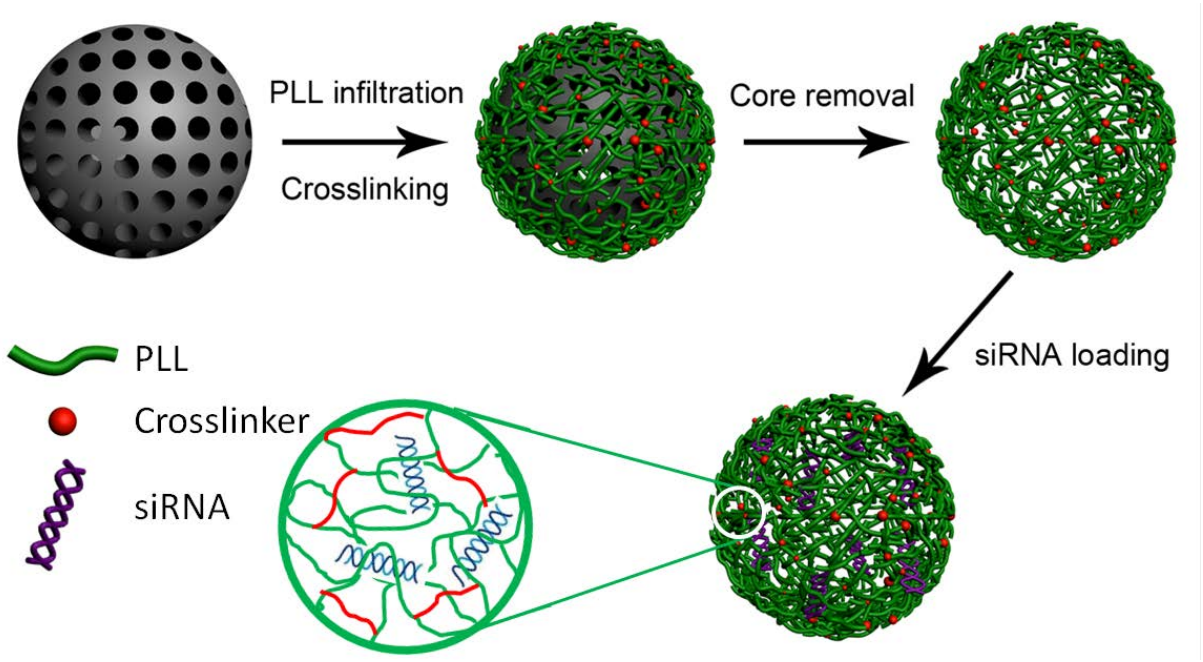

The measured fraction of amine groups was used to determine that the crosslinking degree was 40% (PEG unit/lysine unit), corresponding to 0.0018 mol cm^{-3} density of effective crosslinked chains. These results indicate that a single NPEG-PLL is composed of 27% (w/w) PLL and 73% (w/w) PEG, and the single particle mass, taking into account both polymeric components, amounts to 2.2 pg. The crosslinking reaction concurrently may introduce dangling PEG chains bearing carboxyl groups on the surface of the NPEG-PLLs. The dangling chains are formed when one end of a di-functionalized crosslinking PEG chain does not undergo coupling reaction. This arises during network formation when some functional NHS groups remain unreacted and hydrolyze into carboxyl groups. The potentiometric titration of carboxyl groups (Supporting Information, Figure S2b) present on NPEG-PLL indicates that 5% PEG chains are dangling chains bearing a negative charge.

Physicochemical Characterization of NPEG-PLLs. The diameters of dry NPEG-PLLs (1.4 ± 0.2 μm) and swollen NPEG-PLLs (1.8 ± 0.2 μm) in 0.2 M NaCl were measured by transmission electron microscopy (TEM) (Figure 1a) and confocal microscopy (Figure 1b) analysis, respectively, over a set of 100 particles. The crosslinking degree of NPEG-PLL was also evaluated using microgels swelling measurements and applying the equilibrium swelling theory (developed by Flory and Rehner and modified by Peppas and Merrill[25]), as reported in the Experimental Section. A crosslinks density, $\frac{\upsilon e}{Vo}$, of 0.0016 mol crosslinks cm^{-3} was determined, which is in good agreement with potentiometric titration data. To evaluate porosity, the exclusion properties of NPEG-PLL toward FITC-labeled dextrans (Mw 2000 kDa, R_h=16 nm and 500 kDa, R_h=27 nm) were evaluated by CLSM.[30] After incubation with the two types of FITC-dextran the NPEG-PLLs became fluorescent (Figure 1c), indicating that the NPEG-PLL

nanopores are accessible to 54 nm-sized or smaller macromolecules. In addition, images of swollen NPEG-PLLs acquired using structured illumination super-resolution microscopy (SIM), whose lateral resolution is 100 nm, (Figure 1d) show a highly porous structure. As most of the serum/plasma proteins have a hydrodynamic diameter lower than 25 nm,[31] these results suggest that the NPEG-PLL may be permeable to the proteins during *in vitro* transfection experiments. ζ-potential measurements reveal that the NPEG-PLL surface was positively charged (+20 ± 3 mV) in 10 mM NaCl and slightly negatively charged (-6 ± 2 mV) in PBS. Interestingly, NPEG-PLLs suspended at high concentration in Milli-Q organize in string-like structures[32] (inset Figure 1b). It was recently reported that colloidal particles with a dielectric constant mismatch with the surrounding solvent acquire a dipole moment in a homogeneous external electric (magnetic) field.[32] The resulting dipolar interactions can lead to assembly of the particles into string-like clusters. The uneven crosslinking of NPEG-PLL probably generates a weak permanent dipole that induces a similar assembly of particles in water.

Complexation of siRNA with NPEG-PLLs. The siRNA directed against survivin (siSurv; MW: 13 330 g mol^{-1}) was post-loaded into the crosslinked NPEG-PLL network in phosphate buffer (0.5 x PBS, pH 7.5) using electrostatic interactions. Compared to other methods this procedure would allow the facile mixing of the NPEG-PLL suspension and siRNA prior to patient treatment without any purification steps and with a fine control on particle size distribution.

The nanoporous positively charged polymeric particles provide a scaffold to encapsulate oligonucleotides and other negatively charged biomacromolecules by fast diffusion through the permeable nanoporous structure and *in situ* complexation with the polycation component. In

addition, the co-delivery of siRNA and small molecular weight hydrophobic drugs is feasible by covalent conjugation of drugs to the polymeric backbone of NPEG-PLL.

The siRNA loading into the particles was evaluated by measuring the absorbance at 260 nm of the solutions before and after adsorption, and confirmed by fluorescence microscopy. The N/P ratio (i.e., the ratio of moles of PLL amine groups to RNA phosphate groups) is 18. Due to the nanoporosity and PLL amine groups, NPEG-PLLs show a good adsorption capacity for siSurv (7.5×10^5 molecules per particles). Despite the slightly negative surface charge, the 22-mer siRNA diffuses into the NPEG-PLL nanopores to complex via electrostatic interactions with PLL amine groups. The 22-mer siRNA entangles with the polypeptide chain network, remaining physically entrapped, and is only released after NPEG-PLL deconstruction. After siRNA loading, the NPEG-PLL surface charge measured in 10 mM NaCl did not significantly change (+18 ±5 mV). This indicates that the siRNA chains interact with the inner region of the NPEG-PLL, rather than with the surface.

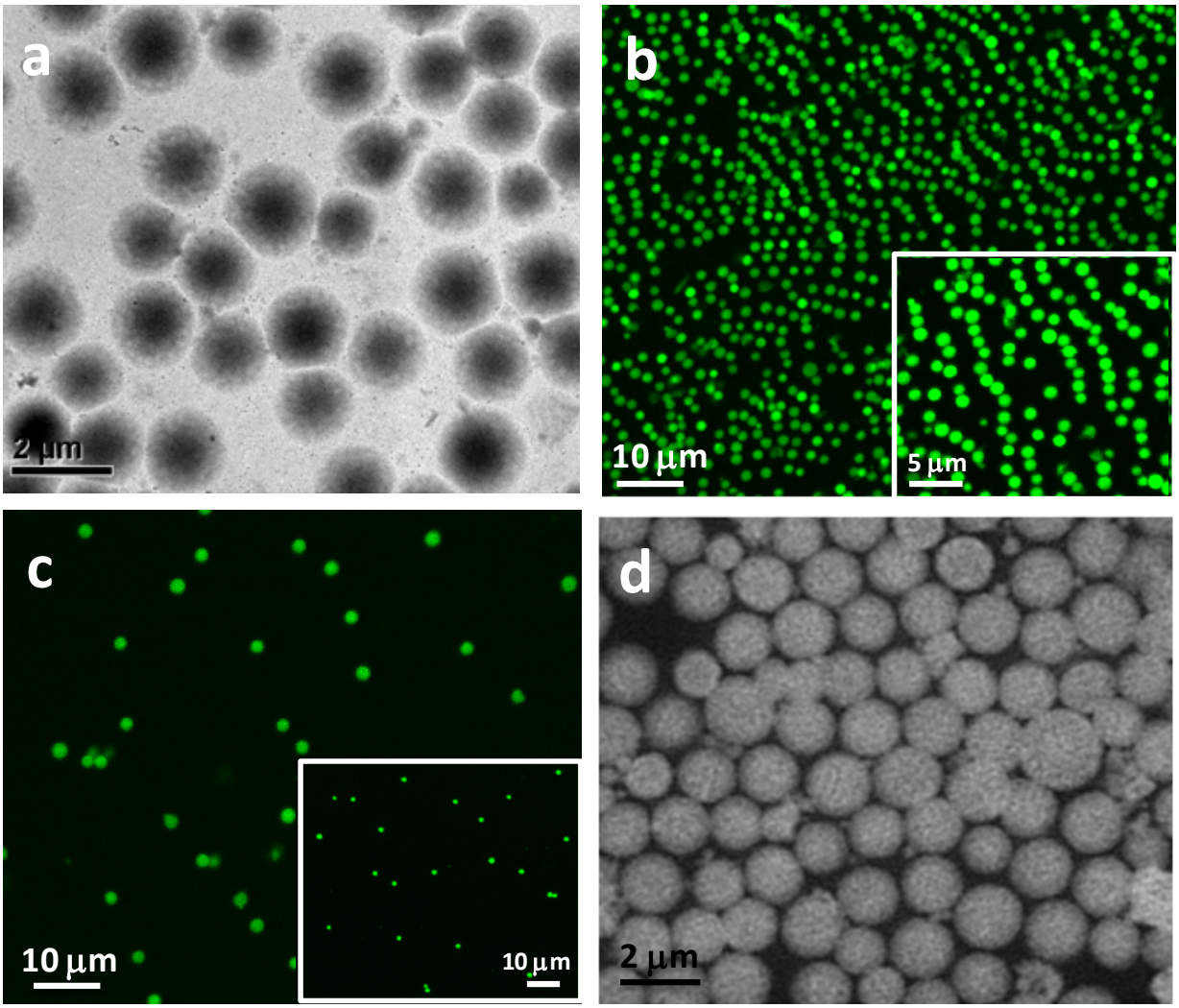

Figure 1. a) TEM images of NPEG-PLLs; b) confocal microscopy image of AF488 NPEG-PLLs in Milli-Q, inset: magnification (×1.5) shows the string-like organization of NPEG-PLLs; c) confocal microscopy image showing diffusion of FITC-dex (2000 kDa) into the NPEG-PLLs, inset: colloidal stability of NPEG-PLLs loaded with AF488-siRNA when incubated with serum proteins at 37 °C for 48 h; d) SIM super-resolution microscopy image of swollen AF488-labeled NPEG-PLLs.

To verify the ability of the NPEG-PLLs to disassemble and release intact siRNA, treatment with the reducing agent (GSH) and proteolytic enzymes (1 mg mL^{-1} protease from *Streptomyces griseus*) was performed. Degradation experiments were performed in 10 mM reduced GSH in PBS solution at 37 °C, mimicking the cytosolic milieu. NPEG-PLLs were fluorescently labeled using AF488 and the fluorescence of the soluble supernatant, after centrifugation of the nondegraded particles, was monitored over 24 h. The complete degradation of NPEG-PLL by GSH occurred within 24 h. Fluorescence emission of the supernatant isolated from a NPEG-PLL suspension, after centrifugation, and exposed to a large excess of GSH (10 mM) in PBS at 37 °C, was analyzed (Supporting Information, Figure S3a). The curve exhibits a plateau indicating the degradation process was completed. This is also corroborated by the absence of residual NPEG-PLL in the vials after centrifugation.

Furthermore, treatment with protease at 37 °C for 8 h caused degradation of the NPEG-PLLs, resulting in a green solution (Supporting Information, Figure S3b). These results confirm that the NPEG-PLLs contain unmodified lysine groups which are known to be the sites of cleavage by proteases such as trypsin.[33] The integrity of siRNA released from NPEG-PLL was studied after protease degradation by measuring the melting temperature of the siRNA duplex (Supporting Information, Figure S4). Specifically, both the released and native siSurv showed comparable melting temperatures (40 °C), indicating that the binding and the disassembly process do not compromise the integrity and stability of the siRNA double strand.

NPEG-PLL Stability in Serum and Plasma. Cationic transfection vectors often display poor efficiency *in vivo* due to their aggregation with negatively charged proteins in serum.[34] Hence, serum/plasma stability of NPEG-PLL loaded with siRNA must be tested to evaluate the application of NPEG-PLLs as a systemic delivery system of siRNA. The NPEG-PLLs retained

their integrity and demonstrated excellent colloidal stability in the presence of plasma proteins at 37 °C for up to 48 h without any change in size or evidence of aggregation (inset Figure 1c). The adsorption of plasma protein on NPEG-PLL surface was verified by ζ-potential measurements. After incubation with human plasma, the NPEG-PLL surface charge became slightly negative (-8 ± 2 mV), indicating an effective surface coverage by a protein corona.

In addition, since plasma proteins are able to diffuse into the NPEG-PLLs and potentially displace siRNA molecules bound to the NPEG-PLL scaffold, we performed experiments aimed at evaluating the capability of plasma proteins to compete with siRNA for electrostatic binding. To this purpose, NPEG-PLLs loaded with AF488-siRNA were incubated in PBS at pH 7.4 containing 10% FBS and 100% human plasma for 3 h and 4 h, respectively. After incubation, the amount of siRNA displaced from NPEG-PLLs by serum proteins was evaluated by quantifying the fluorescent intensity of the supernatant. We found that NPEG-PLLs stably bind siRNA molecules, as only 5% of loaded siRNA was displaced by negatively charged serum proteins. The high PEG content of NPEG-PLLs most likely contributes to the high serum stability by providing a steric shield.

***In Vitro* NPEG-PLL Cell Cytotoxicity and Intracellular Trafficking**. We evaluated the effect of NPEG-PLLs on the viability of PC-3 prostate cancer cells using an MTS assay. Because of its positive charges, a low concentration of PLL (25 μg mL^{-1}) is highly toxic for cells.[33,34] However, survival of PC-3 cells was unaffected upon a 96-h incubation with up to 1000 NPEG-PLL/cell, a particle amount corresponding to a concentration of 44 μg mL^{-1} of NPEG-PLL (Figure 2a). We hypothesize that PLL which has been partly neutralized and immobilized by PEG crosslinking is

advantageous compared with free PLL because the nanoporous structure can shield the polycation-mediated toxicity.

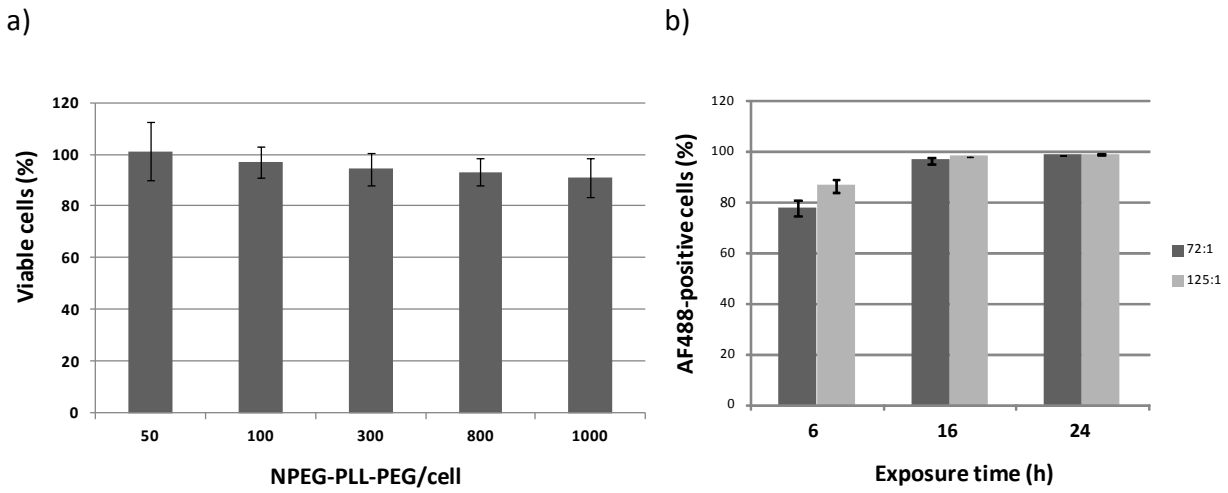

Figure 2. a) Effect of NPEG-PLLs on PC-3 cell survival measured by MTS assay after 96 h incubation. Data are reported as a percentage of viable cells exposed to NPEG-PLLs compared to untreated cells, and represent mean values ± s.d. b) Time-dependent evaluation of NPEG-PLL internalization in PC-3 cells. Cells were exposed to AF488-labeled particles (particles/cell ratio of 72:1 and 125:1) and analyzed by flow cytometry. Data are reported as the percentage of AF488-positive cells. The values represent the mean ± s.d. of at least three independent experiments.

Next, we evaluated the cellular internalization and trafficking of the NPEG-PLLs in PC-3 cells. It has been widely reported that both nano- and micrometer-sized particles are generally internalized by endocytosis and trafficked from early endosomes to lysosomes within the first hours of incubation.[37,38] PC-3 cells were hence incubated with AF488-labeled NPEG-PLLs for different times at 37 °C and, after repeated washing to remove surface bound NPEG-PLLs,

analyzed by flow cytometry (Figure 2b, Supporting Information, Figure S5). The results show a rapid NPEG-PLL uptake in PC-3 cells that occurred within two hours and reached approximately 100% of the overall cell population after 24 h, regardless of the particle/cell ratio. The intracellular trafficking and subcellular destination of the NPEG-PLLs was then investigated by deconvolution microscopy, SIM and FLIM. Deconvolution fluorescence microscopy showed that NPEG-PLLs readily internalized in PC-3 cells (Figure 3), confirming the flow cytometry results. In addition, AF488-labeled NPEG-PLL appeared to be tightly surrounded by lysosomes after internalization, as indicated by the staining for the specific marker LAMP1 (Figure 3a). This would suggest that NPEG-PLLs are effectively internalized by the cells and progressed to acidic environment as they were docked by lysosomes. This observation is consistent with intracellular processing reported for other micrometer-sized particles.[37,38] It is also noted that a fraction of internalized NPEG-PLLs (arrows in Figure 3) were not surrounded by the lysosomal compartment after incubation for 24 h.

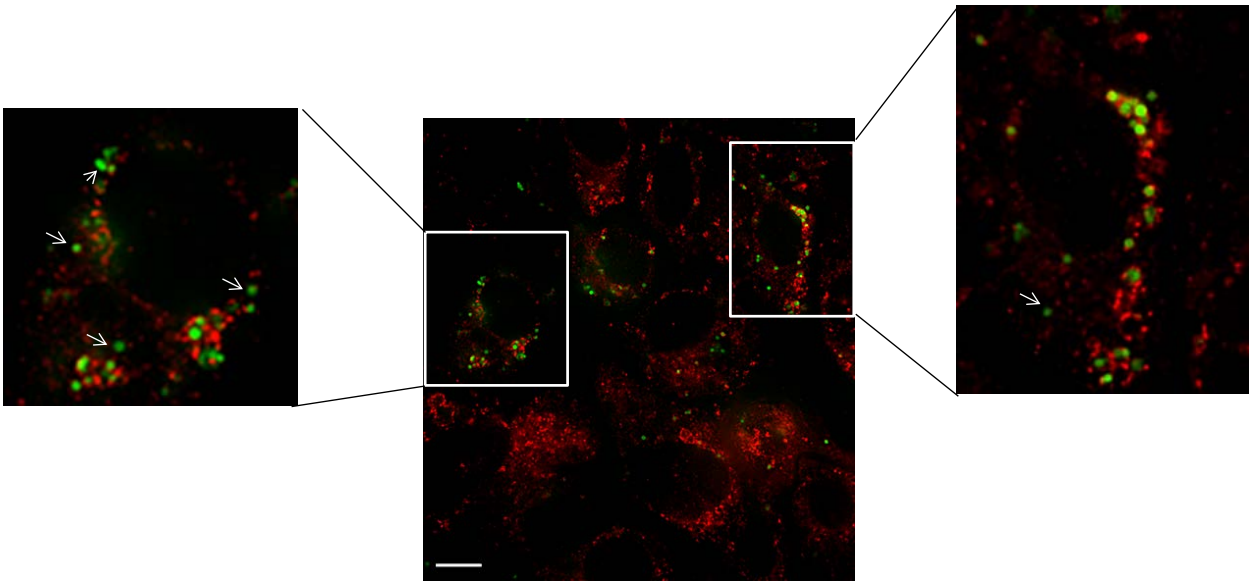

Figure 3. Representative deconvolution microscopy image of PC-3 cells treated with NPEG-PLLs (125:1 particle/cell ratio) for 24 h. After treatment, cells were washed three times with PBS to remove NPEG-PLLs bound to the cell surface. To visualize the lysosomal membrane a LAMP1 antibody was used. NPEG-PLL was labeled with AF488 (green), the lysosome protein LAMP1 was labeled with AF647 Ig-G (red). Scale bars = 10 µm

To gain further insight into the cellular localization of NPEG-PLLs, FLIM studies were performed. For this purpose NPEG-PLLs were labeled with the pH-sensitive fluorophore, FITC, whose fluorescence lifetimes can be used to probe pH.[39] The lifetime difference of internalized NPEG-PLLs is visualized by different colors (from orange to green), thus providing information on the pH changes experienced by NPEG-PLLs. Specifically, the local pH around each particle can be used as an indication of the stage of uptake. To define the pH reference conditions, the FITC fluorescence lifetimes of labeled NPEG-PLLs were first analyzed over a pH range of 5-7. NPEG-PLLs were incubated with PBS at pH 5, 6 and 7, and visualized by FLIM. Figure 4a, b show FLIM images of FITC-labeled NPEG-PLLs acquired at pH 5 and pH 7. Next, PC-3 cells were incubated with FITC-labeled NPEG-PLLs (500 particles/cell) for 2, 7, 24 and 48 h, and analyzed. FLIM images of internalized NPEG-PLLs acquired after 24 h and 48 h incubation are shown in Figure 4c and 4d, respectively. Figure 4c shows the fluorescence emission of internalized NPEG-PLLs with different lifetimes. Average lifetime values were obtained by averaging the lifetimes of 10-20 FITC- NPEG-PLLs taken up in at least 10 cells.

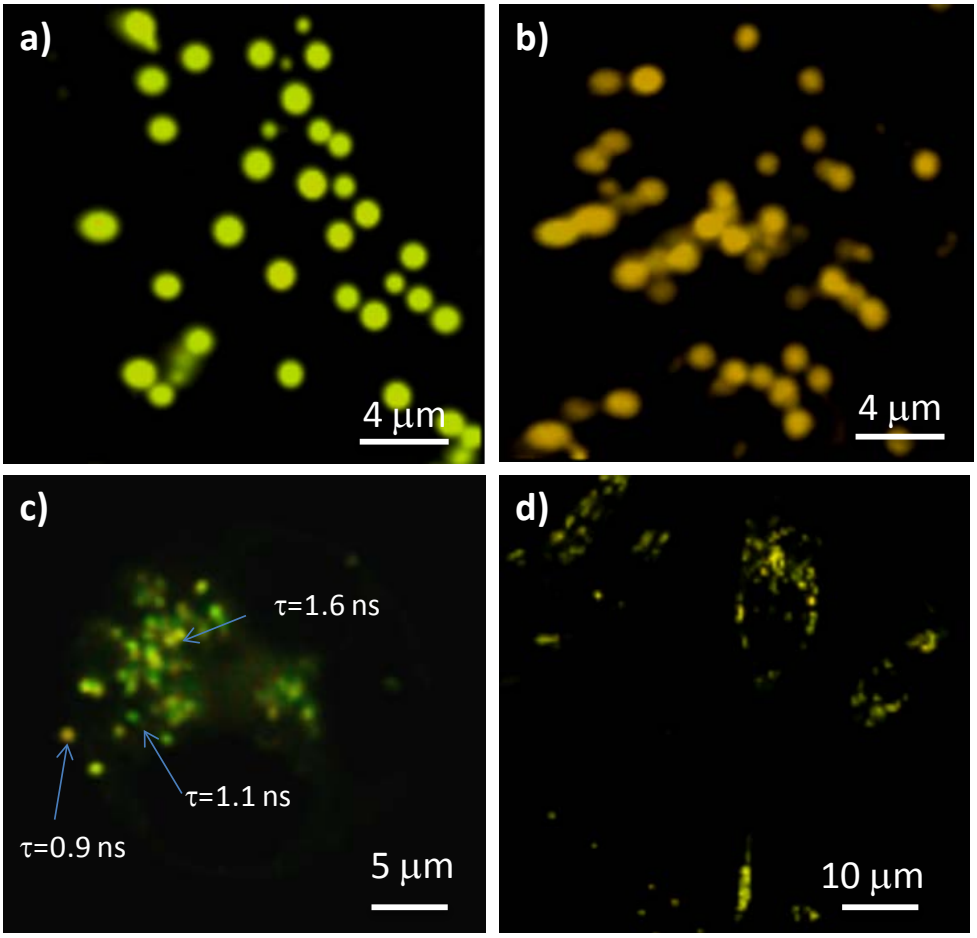

Figure 4. Representative FLIM images of FITC-labeled NPEG-PLLs visualized at a) pH 5 and b) pH 7, as well as upon incubation with PC-3 cells for c) 24 h and d) 48 h. The lifetime difference of internalized NPEG-PLL is clearly visualized by different colors corresponding to different lifetimes.

As reported in Figure 5, fluorescence lifetimes of FITC-labeled NPEG-PLLs changed depending on the cellular environment (e.g., pH). The mean fluorescence lifetimes of NPEG-PLL was 1.8 ns, 1.23 ns and 0.8 ns (Figure 5) at pH 5, 6 and 7, respectively. A previous study on FITC-dextran's lifetimes reported 4 ns at pH 7, and 3 ns at pH 5.[38] However, FITC-PLL shorter lifetimes were observed in other studies[41] and are likely attributed to the fluorescence quenching

induced by the electrostatic interaction between the negatively charged fluorescein moiety and the PLL amine groups. At neutral pH both fluorescein acidic groups OH (pKa = 6.5) and COOH (pKa = 4.2)[42] are able to bind to PLL chains, resulting in significant fluorescence quenching, whereas at pH 5 the protonation of the carboxyl group leads to reduced electrostatic interaction and thus decreased quenching. Static fluorescence spectra of NPEG-PLLs acquired at pH 5 and 7 confirmed the quenching effect observed by FLIM (Supporting Information, Figure S6).

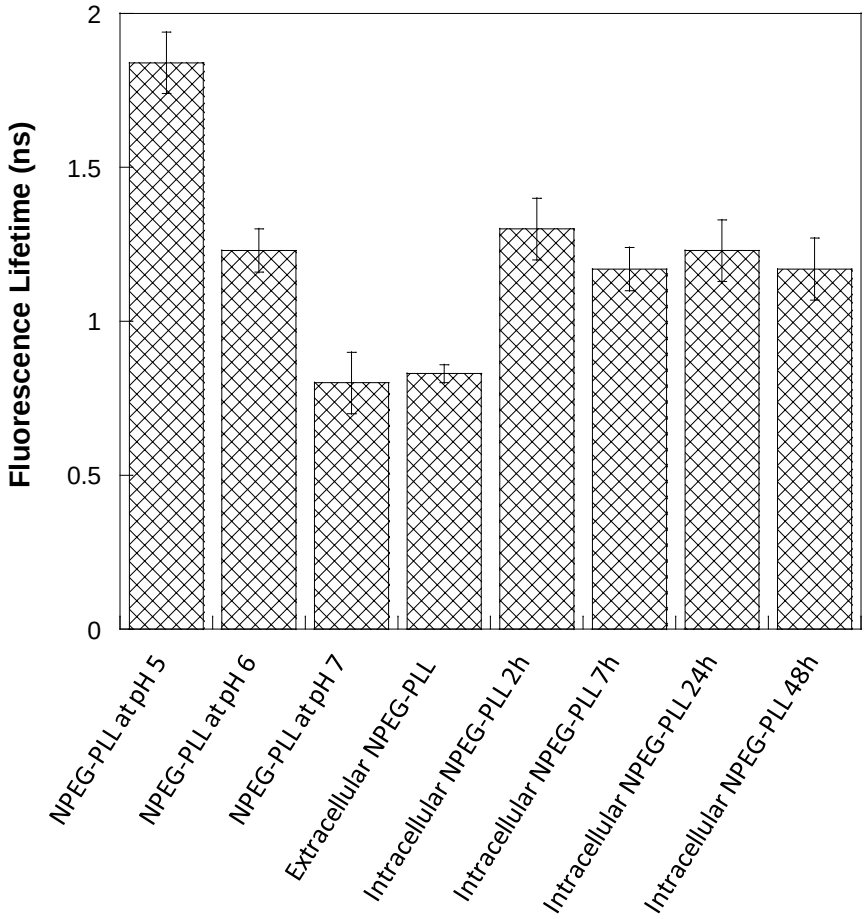

Figure 5: Average fluorescence lifetimes of FITC-labeled NPEG-PLL. PC-3 cells were exposed to FITC-labeled NPEG-PLLs (500 particles/cell) for up to 48 h. After this time period, fluorescence lifetimes were determined and compared to reference FITC-labeled NPEG-PLLs

incubated in PBS at different pH. Each lifetime value was obtained by averaging the lifetimes of 10-20 FITC-labeled NPEG-PLLs taken up in 10 cells.

As reported in Figure 5, the average fluorescence lifetimes of FITC-labeled NPEG-PLL noninternalized observed in the extracellular matrix was 0.9 ns, a value corresponding to that observed at neutral pH. An increase in lifetime from 0.9 to 1.3 ns was observed after 2 h incubation, thus confirming that NPEG-PLLs were readily taken up and is in agreement with flow cytometry data. Overall, the average lifetimes measured for NPEG-PLL after internalization and up to 48 h incubation suggest that NPEG-PLLs are localized in intracellular vesicles at pH 6 from almost the beginning of the uptake process, thus indicating that the particles are likely embedded into vesicular compartments, which may have fused with lysosomes. This finding is in agreement with the deconvolution microscopy imaging analysis. The size of the NPEG-PLLs was monitored during the incubation time and the diameter of NPEG-PLLs decreased from 1.8 to 0.8 μm within 48 h.

The decrease in size as a function of incubation time (Supporting information, Figure S7) indicates that NPEG-PLLs slowly degraded by either lysosomal proteases or reducing agents, eventually completely degrading after 120 h incubation. However, as the redox degradation by GSH occurs in the cytosol, our data suggest that the vesicular compartments wrapping NPEG-PLLs may be leaky and permeable to cytosolic components. It has already been reported that PLL modified with PEG exhibits a cell membrane penetrating effect.[43,44] In addition, cationic amphiphilic peptides with lysine amino acids, are known to induce a pH-independent membrane destabilization by cationic interactions with the endosomal/lysosomal membrane.[45]

SIM imaging with a 3D illumination pattern, 3D-SIM, provided insight into the final fate of NPEG-PLLs at long incubation times (120 h). In comparison with deconvolution and FLIM microscopy, SIM images allow higher particle localization accuracy. Figure 6 shows green fluorescent fragments with a size of approximately 100-200 nm, suggesting NPEG-PLLs degraded over time. In addition, we found no evidence of colocalization between NPEG-PLL or particle debris and lysosomes/late endosomes after 120 h incubation (Figure 6). This confirms either intact NPEG-PLL or particle debris escape the lysosomes/late endosomes and access the cytosol to disassemble and eventually release siRNA.

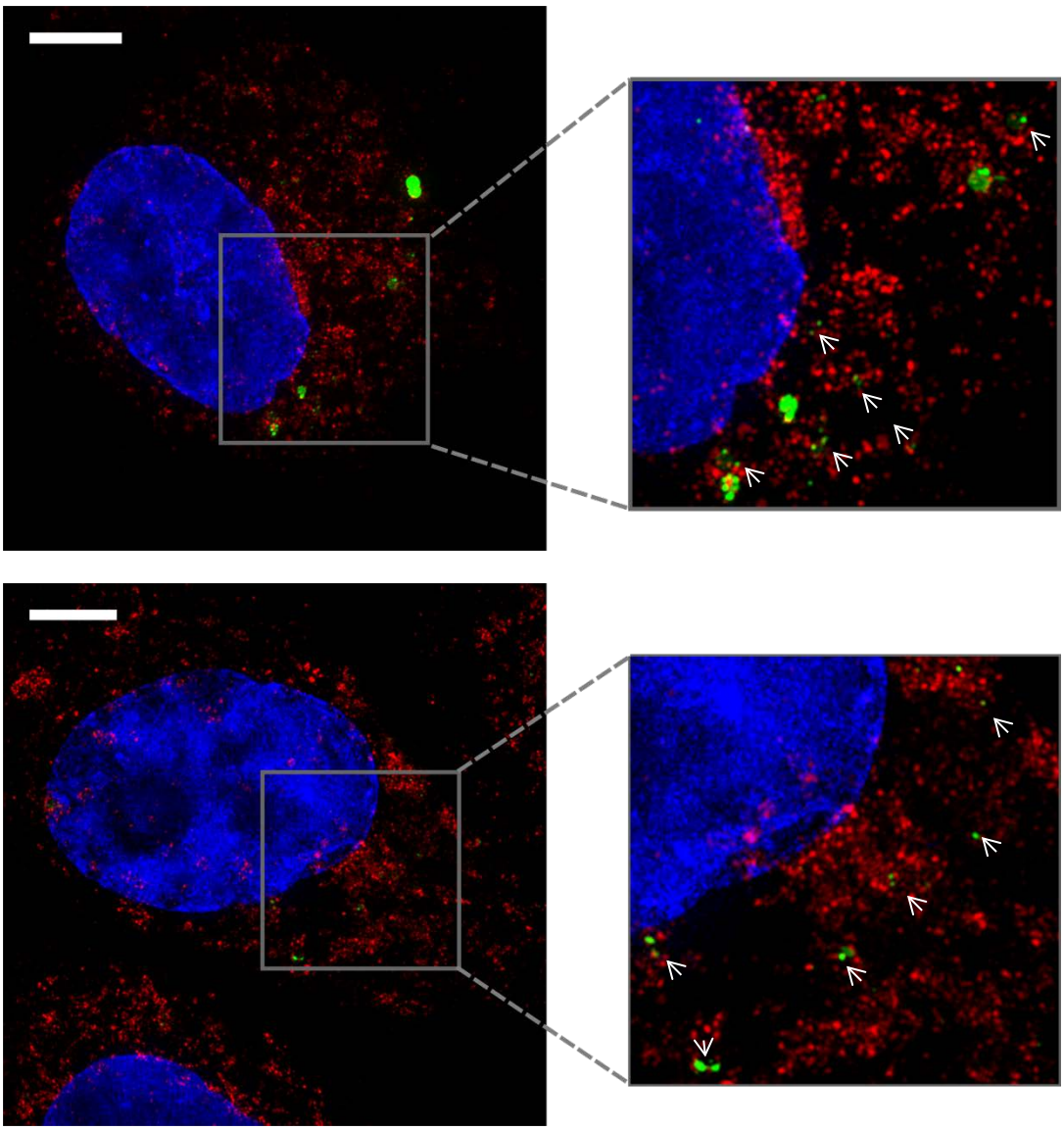

Figure 6. Representative SIM images of AF488-labeled NPEG-PLLs (green) in PC3 cells visualized after 120 h incubation. Lysosomes were immunostained with primary anti-LAMP1 antibody and secondary AF568 Ig-G (red). Nuclei were visualized using Hoechst 33342 (blue). The zoomed region (11 µm x 11 µm) shows green nanometer-sized fluorescent fragments, suggesting NPEG-PLL degradation over time. Maximum intensity projections of cells are shown. Scale bar = 5 µm.

Survivin Silencing by siSurv-Loaded NPEG-PLLs in PC-3 Cells. We next evaluated the ability of NPEG-PLL to deliver a siRNA directed against survivin within PC-3 cells. Specifically, cells were exposed for 72 h to pristine NPEG-PLLs, siScr- and siSurv-loaded NPEG-PLLs (particle/cell ratio of 1000:1; 0.0022 μg/cell). The NPEG-PLL-mediated delivery of the intact siSurv was indirectly evaluated based on the expression levels of the target protein by western immunoblotting. The capability of NPEG-PLLs to deliver siSurv was compared to that of a commercially available cationic lipid-mediated transfer, namely Lipofectamine2000 (LP) (Figure 7). It is noted that safe and efficacious delivery of nucleic acids *in vivo* using Lipofectamine2000 is not feasible due to the toxicity, nonspecific uptake, and undesired immune responses of cationic lipids.[46] LP experiments were performed according to the standard protocol, as previously described.[47] In order to compare LP with NPEG-PLL, cells were exposed to concentrations of siSurv corresponding to the amount delivered with NPEG-PLLs (i.e., 31 nM). As expected, western immunoblotting analysis showed a complete abrogation of survivin expression levels in PC-3 cells exposed to 31 nM LP-siSurv compared to cells exposed to only LP or LP-siScr (Figure 7). Data in Figure 7 suggest a negligible down-modulation of survivin expression levels in cells exposed for 72 h to siSurv-loaded NPEG-PLLs when compared with siScr-loaded particles or pristine NPEG-PLLs (Figure 7a). Chloroquine was also used to enhance cell transfection efficiency of NPEG-PLL by facilitating escape from acidic vesicles within a few hours.[48] Western immunoblotting analyses (Supporting Information, Figure S8) showed a moderate **(**~20%**)** down-regulation of survivin in cells exposed for 72 h to siSurv-loaded particles in the presence of chloroquine compared with cells treated with pristine or siScr-loaded particles. This suggests that chloroquine did not significantly improve the transfection efficiency exerted by NPEG-PLL. Conversely, the exposure of PC-3 cells to siSurv-loaded particles in the

absence of chloroquine for a long incubation period (i.e., 120 h) resulted in a marked down-modulation (~59 ± 8%, $P<0.05$) of the protein compared with cells exposed to empty or siScr-loaded NPEG-PLLs (Figure 7b), thus suggesting the successful, although delayed, delivery of the bioactive siRNA. NPEG-PLL exhibited slightly lower levels of transfection than Lipofectamine2000.

We speculate that the slow release of siRNA to the target site depends on the slow redox cleavage of disulfide bonds of NPEG-PLL. The large number of NPEG-PLLs internalized by PC-3 cells may exhaust the available glutathione and consequently multiple cellular division of cells is required to complete the redox deconstruction of NPEG-PLLs. Overall, our results suggest that NPEG-PLLs not only protect siSurv from degradation, but also make it accessible to the cytosolic target site in its active form, even if only after relatively long-term exposure.

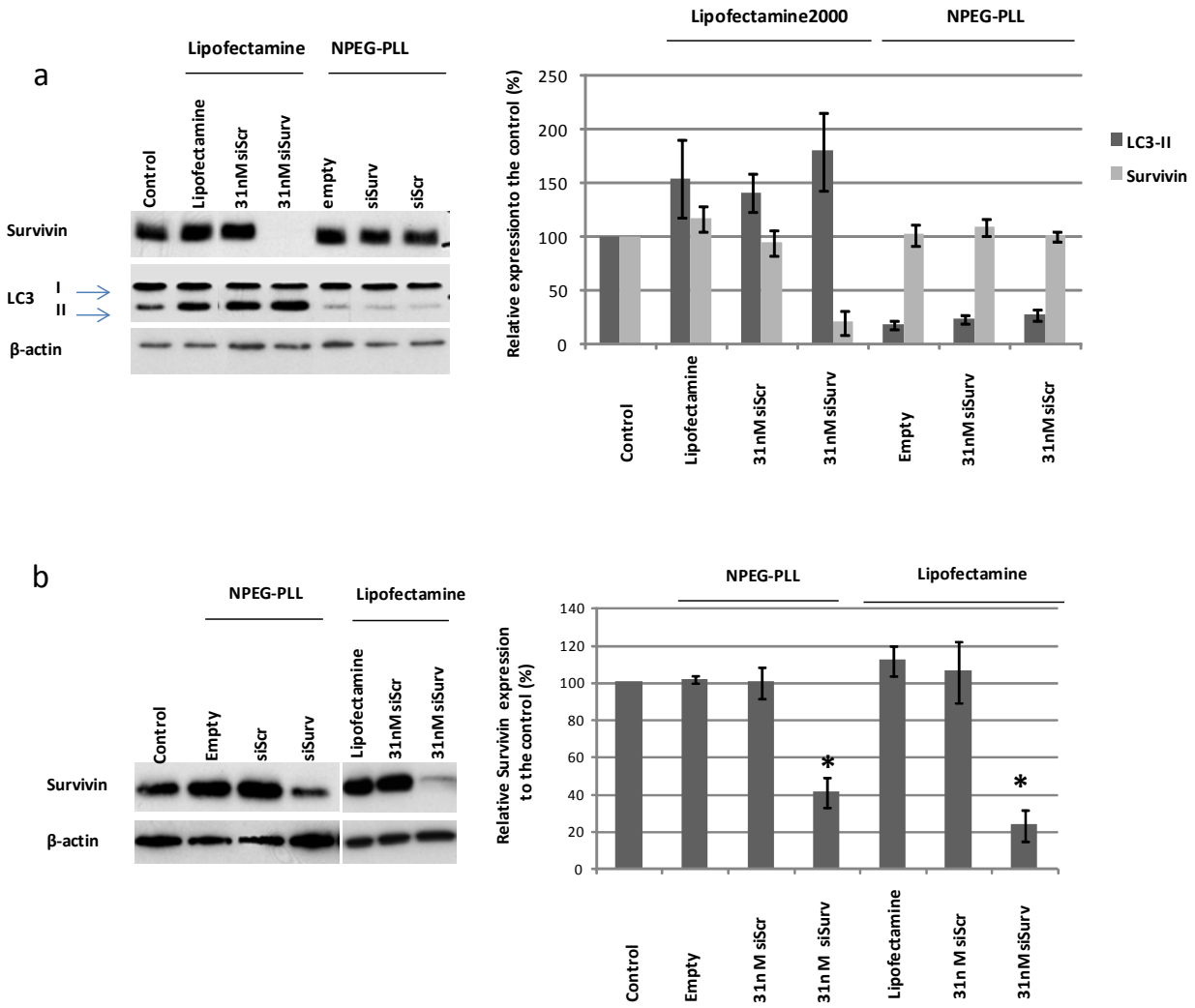

Figure 7: Representative Western immunoblot showing survivin and LC3 expression levels in PC-3 cells exposed to siSurv (31 nM) using either LP or siSurv-loaded NPEG-PLLs. PC-3 cells were treated with NPEG-PLLs (1000 particles/cell) for a) 72 h and b) 120 h. β-actin was used as the control for protein loading. The histograms on the right show the quantification of the relative expression of survivin and LC3 II normalized toward β-actin and compared to the untreated control. The values represent the mean ± s.d. of three independent experiments.

The values represent mean ± s.d. of three independent experiments. *P<0.05 (ANOVA) NPEG-PLL-siSurv versus NPEG-PLL-siScr, NPEG-PLL-empty and Control, and 31 nM siSurv versus lipofectamine and siScr.

A number of recent studies suggest that redox-active particles undergo autophagic sequestration in PC-3 cells.[47,49] To gain insight into the possible autophagosome formation as a response of PC-3 cells to NPEG-PLL internalization, the conversion of the LC3 protein in PC-3 cells from the cytosolic (LC3-I) to the autophagosome-associated (LC3-II) was assessed by Western immunoblotting. As shown in Figure 7a, an induction of LC3-II was evidenced in PC-3 cells transfected with LP alone or in the presence of siRNA (50-100% induction in comparison to untreated cells). Conversely, the lack of conversion of LC3-I to LC3-II in cells treated with pristine NPEG-PLLs (Figure 7a) indicates that prostate cancer cells exposed to redox-active NPEG-PLLs did not elicit a cell defense response, as instead observed in the same cell experimental model exposed to other redox-active capsules.[47]

This result indicates that siSurv-loaded NPEG-PLLs or smaller fragments reach the cytosolic target and significantly suppress survivin expression, which in turn may only occur if the NPEG-PLL has access to the cytosol by escaping lysosomal degradation. However, it should be taken into account that siSurv-loaded NPEG-PLL-mediated down-modulation of the target gene is the end-point of an intracellular cascade, of which endo-lysosomal escape is only one step. The dissociation of the cargo from its carrier and the cytosolic translocation of the siRNA to the apparatus driving the RNA interference process are crucial steps that can affect the final outcome.

Our data also show that siSurv-dependent down-regulation of survivin did not result in any remarkable interference with the proliferation/viability of PC-3 cells (Figure 8). This evidence is in agreement with previous findings indicating that survivin down-regulation *per se* is not always able to induce tumor cell death, rather it contributes to enhancing the antitumor activity of radiation and/or chemotherapeutic agents.[50,51] Based on these observations, the activity of a subtoxic concentration (30 nM, see control in Figure 8) of paclitaxel, an anticancer agent acting as mitotic inhibitor, was assessed. Specifically, the exposure of PC-3 to paclitaxel alone or in association with empty or siScr-loaded particles, did not significantly affect the viability of prostate cancer cells, whereas a significant ($P<0.05$) impairment of cell survival was observed in cells concomitantly exposed to the drug and siSurv-loaded particles (Figure 8).

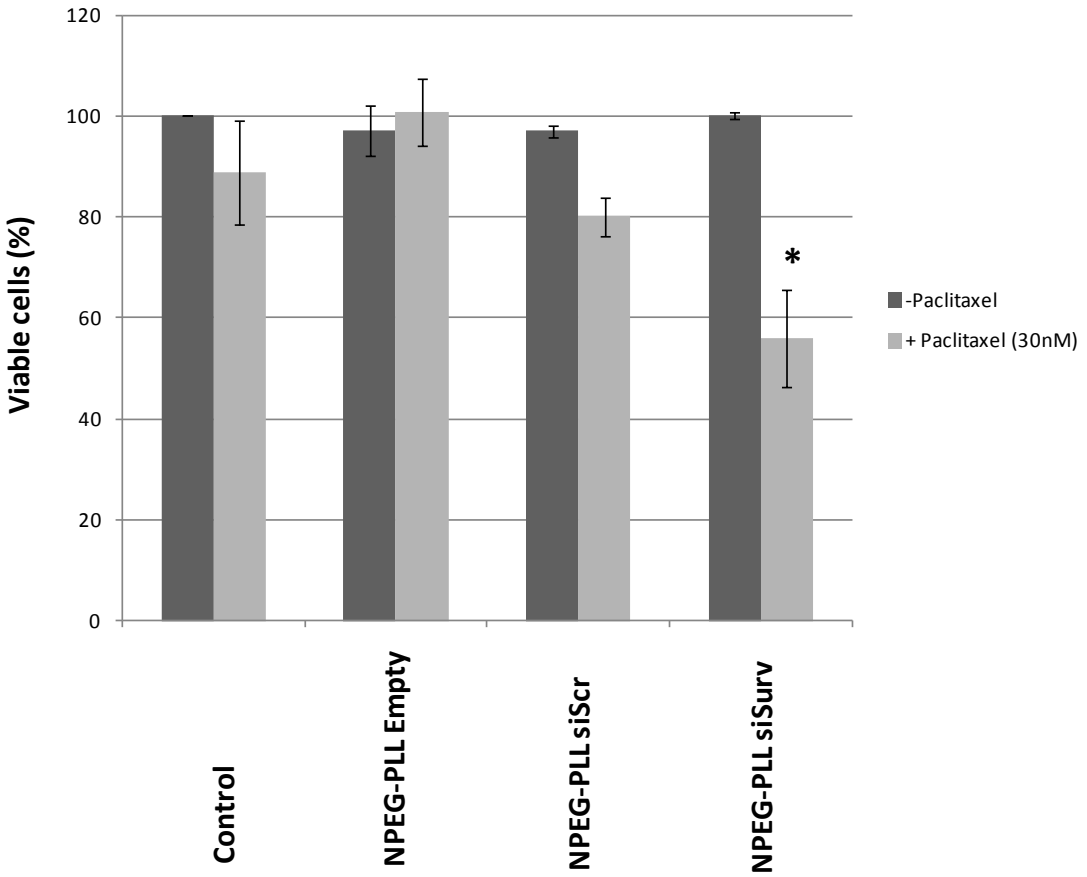

Figure 8. Effect of paclitaxel on PC-3 cell survival exposed for 120 h to pristine particles, siScr- and siSurv-loaded NPEG-PLLs (1000 particles/cell) measured by MTS assay. After 72 h treatment with particles, paclitaxel (30 nM) was added for a further 48 h. Data are reported as a percentage of viable cells in treated compared to untreated cells and represent mean values ± s.d. *P<0.05 (ANOVA) NPEG-PLL-siSurv versus NPEG-PLL-siScr, NPEG-PLL-empty and Control.

These data indicate that the exposure of PC-3 cells to siSurv-NPEG-PLLs and paclitaxel results in an increased cytotoxic activity of the anticancer drug as a consequence of the combination of the action of paclitaxel on microtubule (mitotic arrest) and abrogation of survivin expression

levels (a survival factor). Such enhanced cytotoxic activity of paclitaxel in the presence of abrogated survivin expression levels obtained by using NPEG-PLLs is expected to result in reduced drug-dependent side effects, important when considering the dramatic side effects associated with the use of paclitaxel in the chemotherapeutic regimens.

3. Conclusions

NPEG-PLLs were engineered as redox-responsive and highly loaded depots, which allowed the sustained release of siRNA, leading to effective silencing of the target gene in prostate cancer cells. Our data show that the NPEG-PLLs are readily internalized by prostate cancer cells and exhibit no cytotoxicity or perturbations of the intracellular milieu (i.e., off-target effects) in cells exposed to high doses of empty redox-active NPEG-PLLs. The internalized particles were processed from endosomes to acidified compartments (pH 6) and degraded within 120 h in the cytosol. Our data showed a remarkable reduction in survivin amounts only upon a 120 h incubation of prostate cancer cells with siSurv-loaded NPEG-PLLs. However, only a low dose of surv-siRNA (30nM) is necessary to significantly silence the target gene. Finally, an enhanced and synergistic antitumor activity of a subtoxic dose of paclitaxel was observed when combined with the siSurv-NPEG-PLL-dependent down-regulation of the pro-survival factor survivin.

Translation of this promising nanoporous siRNA carrier from *in vitro* to *in vivo* models is envisaged. Further efforts are being made for testing nanometer sized NPEG-PLL porous particles in tumor-bearing mice models. To prolong circulation time and exploit the enhanced permeability and retention effect, nanometer sized porous silica template will be used to construct NPEG-PLLs.

This work paves the way for a further exploration of the co-delivery of chemotherapeutic drugs and siRNA within the single vector NPEG-PLL as a rational strategy for combined cancer therapy.

Supporting Information. Figure S1 (chemical structure of the NPEG-PLL), Figure S2 (potentiometric titration of NPEG-PLL), Figure S3 (degradation of NPEG-PLL by GSH and protease),Figure S4 (melting curve of native and released siRNA), Figure S5 (flow cytometric profiles of PC-3 cells treated with NPEG-PLL), Figure S6 (fluorescence spectra of NPEG-PLL), Figure S7. (intracellular degradation of NPEG-PLL), Figure S8 (WB showing survivin expression levels in PC-3 cells treated with NPEG-PLLs and chloroquine). This material is available free of charge via the Internet at http://pubs.acs.org.

AUTHOR INFORMATION

Corresponding Author

* E-mail: fcaruso@unimelb.edu.au (Frank Caruso)

* E-mail: nadia.zaffaroni@istitutotumori.mi.it (Nadia Zaffaroni)

Author Contributions

All authors contributed to the manuscript. All authors have given approval to the final version of the manuscript.

ACKNOWLEDGMENT

This work was supported in part by grants from the Marie Curie Actions – International Research Staff Exchange Scheme (Grant #247542, Nanosirna), Fondazione Italo Monzino, and

by the Australian Research Council (ARC) under the Australian Laureate Fellowship (F. Caruso, FL120100030), Super Science Fellowship (F. Caruso, FS110200025), ARC Centre of Excellence in Convergent Bio-Nano Science and Technology (Project Number CE140100036), and Future Fellowship 2014 (F. Cavalieri FT140100873) schemes. The authors thank Benjamin Hibbs and Matthew Faria for providing assistance in the use of SIM and protein data bank, respectively. This work was performed in part at the Materials Characterisation and Fabrication Platform (MCFP) at The University of Melbourne.

REFERENCES

(1) Thomas, C. E.; Ehrhardt, A.; Kay, M. A. *Nat. Rev. Genet*. **2003**, *4*, 346–358.

(2) Burnett, J. C.; Rossi, J. J. *Chem. Biol*. **2012**, *19*, 60–71.

(3) Samarasinghe, R. M.; Gibbons, J.; Kanwar, R. K.; Kanwar, J. R. *Expert Opin. Drug Discov.* **2012**, *7*, 1083–1092.

(4) Cheng, Z. L.; Al Zaki, A.; Hui, J. Z.; Muzykantov, V. R.; Tsourkas, A. *Science* **2012**, *338*, 903–910.

(5) Oyewumi, M. O.; Kumar, A.; Cui, Z. *Expert Rev. Vaccines* **2010**, *9*, 1095–1107.

(6) Edwards, D; Ben-Jabria, A; Langer, R. *J. Appl. Physiol*. **1998**, *84*, 379–385.

(7) Oe, Y.; Christie, R. J.; Naito, M.; Low, S. A.; Fukushima, S.; Toh, K.; Miur, Y.; Matsumoto, Y.; Nishiyama, N.; Miyata, K.; Kataoka, K. *Biomaterials* **2014,** *35*, 7887–7895.

(8) Nelson, C. E.; Kintzing, J. R.; Hanna, A.; Shannon, J. M.; Gupta, M. K.; Duvall, C. L. *ACS Nano* **2013**, *10*, 8870–8880.

(9) Gao, Y.; Wang, Z-Y.; Zhang, J.; Zhang, Y.; Huo, H.; Wang, T.; Jiang, T.; Wang, S. *Biomacromolecules* **2014**, *15*, 1010–1018.

(10) Han, L.; Tang, C.; Yin, C. *Biomaterials* **2014**, *35*, 7978–7991.

(11) Yang, F.; Huang, W.; Li, Y.; Liu, S.; Jin, M.; Wang, Y.; Jia, L.; Gao, Z. *Biomaterials* **2013**, *34*, 5689–5699.

(12) He, C.; Lu, K.; Liu, D.; Lin, W. *J. Am. Chem. Soc*. **2014**, *136*, 5181−5184.

(13) Rettig, G. R.; Behlke, M. A. *Mol. Ther*. **2012**, *20*, 483–512.

(14) Tamura, A.; Oishi, M.; Nagasaki, Y. *J. Controlled Release* **2010**, *146*, 378–387.

(15) Zhu, L.; Perche, F.; Wang, T.; Torchilin, V. P. *Biomaterials* **2014**, *35*, 4213−4222.

(16) Aliabadi, H.M.; Landry B.; Mahdipoor P.; Uluda_H. *Mol. Pharmaceutics* **2011**, *8*, 1821–1830.

(17) Aliabadi, H.M.; Landry B.; Sun, C.; Tang, T.; Uluda_H. *Biomaterials* **2012**, *33*,2546–2569.

(18) Wang, Y. J.; Yu, A. M.; Caruso, F. *Angew. Chem. Int. Ed*. **2005**, *44*, 2888−2892.

(19) Cui, J.; De Rose, R.; Best, J. P.; Johnston, A. P. R.; Alcantara, S.; Liang, K.; Such, G. K.; Kent, S. J.; Caruso, F. *Adv. Mater.* **2013**, *25*, 3468−3471.

(20) Cui, J.; Yan, Y.; Wang, Y.; Caruso, F. *Adv. Funct. Mater.* **2012**, *22*, 4718−4723.

(21) Richardson, J. J.; Maina, J. W.; Ejima, H.; Hu, M.; Guo J.; Choy, M. Y.; Gunawan, S. T.; Lybaert, L.; Hagemeyer, C. E.; De Geest, B. G.; Caruso, F. *Adv. Sci.* **2015**, 2, 1400007.

(22) Coumar, M. S.; Tsai, F. Y.; Kanwar, J. R.; Sarvagalla, S.; Cheung, C. H. A. *Canc. Treat. Rev.* **2013**, *39*, 802–811.

(23) Li, F.; Ambrosini, G.; Chu, E. Y.; Plescia, J.; Tognin, S.; Marchisio, P. C.; Altieri, D. C. *Nature* **1998**, *10*, *396*, 580−584.

(24) Pennati, M.; Folini, M.; Zaffaroni, N. *Expert Opin. Ther. Targets* **2008**, *12*, 463–476.

(25) Echeverria, C.; Peppas, N. A.; Mijangos, C. *Soft Matter*, **2012**, *8*, 337–346.

(26) Saunders, B.; Vincent, B. Responsive Microgel Dispersions. In Encyclopedia of Surface and Colloid Science, 2nd edition, Somasundaran P.; CRC Press Taylor & Francis Group, Boca Raton, US, **2006**; Vol.7, p.5435.

(27) Merrill, E. W.; Dennison, K. A; Sung, C. *Biomaterials* **1993**, *14*, 1117−1126.

(28) Laemmli, U. K. *Nature* **1970**, *227*, 680−685.

(29) Cheng, R.; Feng, F.; Meng, F.; Deng, C.; Feijen, J.; Zhong, Z. *J. Controlled. Release* **2011**, *152*, 2−12.

(20) Armstrong, J. K.; Wenby, R. B.; Meiselman, H. J.; Fisher, T. C. *Biophys. J.* **2004**, *87*, 4259–4270.

(31) Abola, E. E.; Bernstein, F. C.; Bryant, S. H.; Koetzle, T. F.; Weng, J. **1987**. Protein Data Bank.

(32) Orlin, D. V.; Gupta, S. *Adv. Mater*. **2009**, *21*, 1897–1905.

(33) Yui, S.; Osawa, Y.; Ichisugi, T.; Kamata, R. M. *Mediators Inflamm.* **2014**, *2014*, 971409.

(34) Alexis, F.; Pridgen, E.; Molnar, L. K.; Farokhzad, O. C. *Mol. Pharm.* **2008**, *5*, 505−515.

(35) Zhou, Z.; Shen, Y.; Tang, J.; Fan, M.; Van Kirk, E. A; Murdoch, W. J.; Radosz, M. *Adv. Funct. Mater.* **2009**, *19*, 3580–3589.

(36) Fischer, D.; Li, Y.; Ahlemeyer, B.; Krieglstein, J.; Kissel, T. *Biomaterials* **2003**, *24*, 1121−1131.

(37) Yan, Y.; Lai, Z. W.; Goode, R. J.; Cui, J.; Bacic, T.; Kamphuis, M. M. J.; Nice, E. C.; Caruso, F. *ACS Nano* **2013**, *7*, 5558−5567.

(38) Meng, H.; Yang, S.; Li, Z.; Xia, T.; Chen, J.; Ji, Z.; Zhang, H.; Wang, X.; Lin, S.; Huang, C.; Zhou, Z. H.; Zink, J. I.; Nel, A. E. *ACS Nano* **2011,** *5*, 4434−4447.

(39) Han, J.; Burgess, K. *Chem. Rev*. **2010,** *12*, 2709−2728.

(40) Lin, H-J.; Herman, P.; Lakowicz, J. R. *Cytometry Part A* **2003,** *52A*, 77–89.

(41) Lakowicz, J. R. Fluorescence Sensing. In Principles of Fluorescence Spectroscopy, 3rd ed; Springer: Baltimore US, **2006**, 19, p 634.

(42) Frech, T.; So, P. T. C.; Weaver, D. J.; Coelho-Sampaio, T., Gratton, E., Voss, E. W.; Carrero, J. *J. Microsc.* **1997**, *185*, 339−353.

(43) Choi, Y. H.; Liu, F.; Kim, J. S.; Choi, Y. K.; Park, J. S.; Kim, S. W. *J. Controlled Release* **1998**, *54*, 39−48.

(44) Luhmann, T.; Rimann, M.; Bittermann, A. G.; Hall, H. *Bioconjugate Chem.* **2008,** *19*, 1907−1916.

(45) Martens, T. F.; Remauta, K.; Demeester, J.; De Smedt, S. C.; Braeckmansa, K. *Nano Today* **2014**, *9*, 344−364.

(46) Uchida, S.; Itaka, K.; Uchida, H.; Hayakawa, K.; Ogat, T.; Ishii, T.; Fukushima, S.; Osada, K.; Kataoka, K. *PLoS One* **2013**, *8*, e56220.

(47) Becker, A. L.; Orlotti, N. I.; Folini, M.; Cavalieri, F.; Zelikin, A. N.; Johnston, A. P. R.; Zaffaroni, N.; Caruso, F. *ACS Nano* **2011**, *22*, 1335−1344.

(48) Khalil, A.; Kogure, K.; Akita, H.; Harashima, H. *Pharmacol. Rev.* **2006**, *58*, 32−45.

(49) Beretta, G. L.; Folini, M.; Cavalieri, F.; Yan, Y.; Fresch, E.; Kaliappan, S.; Hasenöhrl, C.; Richardson, J. J.; Tinelli, S.; Fery, A.; Caruso, F.; Zaffaroni, N. *Nanoscale* **2015**, *7*, 6261.

(50) Pennati, M.; Binda, M.; Colella, G.; Folini, M.; Citti, L.; Villa, R.; Daidone, M. G.; Zaffaroni, N. *J. Invest. Dermatol.* **2003**, *120*, 648−654.

(51) Pennati, M.; Binda, M.; Cesare, M. De; Pratesi, G.; Folini, M.; Citti, L.; Daidone, M. G.; Zunino, F.; Zaffaroni, N. *Carcinogenesis* **2004**, *25*, 1129−1136.

Table of Contents Graphic and Synopsis

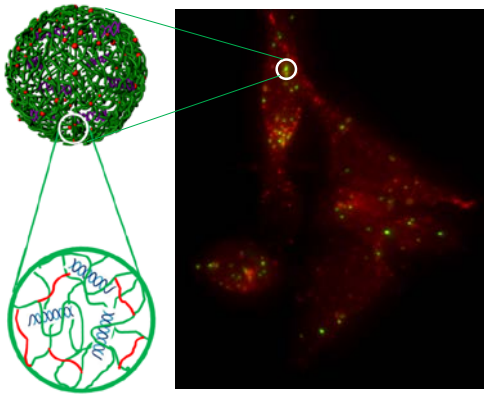

Nanoporous poly(ethylene glycol)-poly-L-Lysine particle are engineered as redox-responsive, degradable and highly loaded depots, which allow the sustained release of siRNA, leading to effective silencing of survivin gene expression in prostate cancer cells.